Theoretical and Experimental Investigations of Thermoresistive Micro Calorimetric Flow Sensors Fabricated by CMOS MEMS Technology

Wei Xu, Kui Song, Shenhui Ma, Bo Gao, Yi Chiu, *Member, IEEE*, and Yi-Kuen Lee, *Member, IEEE*

***Abstract*— A general 1-D model was presented to predict the characteristics of CMOS thermoresistive micro calorimetric flow (TMCF) sensor with two types of packaging, i.e., open-space type and channel type, for both gases and liquids. The 1-D model was first validated by a numerical computational fluid dynamics (CFD) model and was subsequently normalized for different fluids flow. Notably, the model proposed by Nguyen and Dötzel is a special case of our 1-D model. The normalized output of TMCF sensor is a function of normalized input parameters of Reynolds number Re and Prandtl number Pr. The scaling analysis of the sensor output, sensitivity, and power consumption was performed to optimize the design of TMCF sensors in terms of key design parameters, including the thin film thickness, the height of bottom cavity, and so on. Accordingly, three pairs of TMCF sensors were designed and fabricated by using a 0.35 μm 2P4M CMOS microelectromechanical systems technology. The fabricated sensors showed a normalized sensitivity of 230 mV/(m/s)/mW for nitrogen gas flow, which was two orders of magnitude higher than the previous CMOS flow sensors. Therefore, the proposed 1-D model is a promising tool for the sensor's system-level design with the on-chip microelectronics for the Internet of Things. [2016-0098]**

***Index Terms*— 1-D sensor model, CMOS microelectromechanical systems (MEMS), Thermoresistive, Micro calorimetric flow sensor, Prandtl number, Reynolds number.**

I. Introduction

THE MEASUREMENT of fluids flow is crucial for industrial and biomedical applications. Conventional flow measurement instruments are usually bulky and expensive. After the first silicon-based micro flow sensor was reported in 1974 [1], many micro flow sensors have been proposed for a variety of physical principles and fluids [2]–[5]. These micro flow sensors demonstrated diverse applications, including biomedical instrumentation [6], demand control ventilation systems [7], spacecraft propulsion systems [8], and so on.

The majority of micro flow sensors can be classified as either thermal or non-thermal, depending on the mode of operation. Particularly, different types of thermal flow sensors have been presented [3]–[5], such as hot-wire/hot-film, calorimetric, time-of-flight. However, few of these thermal flow sensors were developed with the CMOS MEMS technology. To date, mature CMOS fabrication processes are available in many IC foundries. It should be cost-effective to leverage these existing CMOS fabrication techniques to implement the MEMS flow devices with the highly integrated circuits (ICs) and micro mechanical components [9]. In practice, thermal flow sensors do not require any moving parts; this makes them perhaps the easiest flow measurement devices to be implemented in CMOS process due to their structural and electronic simplicity.

In addition to the microfabrication technology, limited work has been conducted to investigate the effect of sensor structures and dimensions on the key merits of the thermal flow sensors, such as sensitivity, and power consumption, etc. One exception is that Mayer *et al.* [10] fabricated the CMOS gas flow sensors by using the micro thermopile transducers and experimentally investigated the dependence of device output on the design parameters and flow channel dimensions. To the best of our knowledge, there is no satisfactory 1D model to predict the responses of thermoresistive micro calorimetric flow (TMCF) sensors to the input flow of gases and liquids. In comparison with the time-consuming CFD models, 1D model can provide much more efficient device optimization and microsystem integration: micro thermal flow sensors with integrated microelectronics for the Internet of Things (IoT).

As summarized in Table I, several calorimetric flow sensor models have been presented in past decades. Komiya *et al.* [11] developed an analytical model to describe the heat transfer in an electrically heated capillary. Afterward, Lammerink *et al.* [12] presented a model for a free-standing sensor structure within a micro flow channel, which was essentially the same as the one developed by Komiya. Nguyen and Dötzel [13] improved Lammerink's model to a sensor model for the nonintrusive thin film structure. However, both Lammerink and Nguyen assumed a thermal boundary condition of ambient temperature T_a at infinity

Manuscript received May 7, 2016; revised July 11, 2016; accepted July 24, 2016. Date of publication August 11, 2016; date of current version September 29, 2016. This work was supported in part by the Hong Kong Research Grant Council under Grant 16205314 and in part by Hong Kong ITF under Grant ITS/112/16FP. Subject Editor L. Lin.

W. Xu, K. Song, and Y.-K. Lee are with the Department of Mechanical and Aerospace Engineering, Hong Kong University of Science and Technology, Hong Kong (e-mail: wxuaf@connect.ust.hk; songkui-25@163.com; meyklee@ust.hk).

S. Ma is with the Department of Mechanical and Aerospace Engineering, Hong Kong University of Science and Technology, Hong Kong, and also with the Department of Microelectronics, Xi'an Jiaotong University, Xi'an 710049, China (e-mail: smaae@connect.ust.hk).

B. Gao is with the Division of Biomedical Engineering, Hong Kong University of Science and Technology, Hong Kong (e-mail: bgaoaa@connect.ust.hk).

Y. Chiu is with the Department of Electrical and Computer Engineering, National Chiao Tung University, Hsinchu 300, Taiwan (e-mail: yichiu@mail.nctu.edu.tw).

Color versions of one or more of the figures in this paper are available online at http://ieeexplore.ieee.org.

Digital Object Identifier 10.1109/JMEMS.2016.2596282

TABLE I
SUMMARY OF THE REPORTED CALORIMETRIC FLOW SENSOR MODEL

References	Models
Komiya[11,a]	$KA\frac{d^2\theta}{dz^2}-Q\frac{d\theta}{dz}-\mu\theta+i^2R=0$
Lammerink[12,b]	$k_f\frac{d^2T(x)}{dx^2}-\rho C_pU\frac{dT(x)}{dx}-\frac{k_fT(x)}{l_z^2}=0$
Nguyen[13,c]	$\left(\frac{1}{2}k_f\delta_t+k_st\right)\frac{d^2T(x)}{dx^2}-\frac{1}{2}\rho C_pU\delta_t\frac{dT(x)}{dx}-\frac{k_fT(x)}{\delta_t}=0$

[a] Pipe flow: μ = heat loss coefficient, which was determined by experiments.
[b] Channel flow: l_z = half height of the flow channel.
[c] Channel flow: δ_t = thickness of thermal boundary layer, which was assumed as channel height.

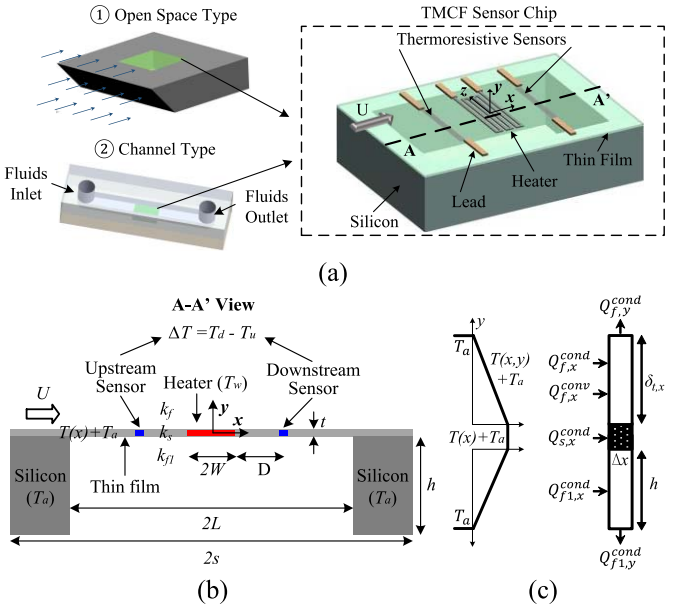

Fig. 1. (a) Two types of TMCF sensor packaging: open-space type and channel-type, (b) Schematic of a general 1D TMCF sensor model with the input velocity (U) and sensor output $\Delta T = T_d - T_u$, (c) Temperature profile in the y direction and the control volume of $\Delta x \times y \times 1$ (excluding the micro heater region) for heat flux analysis.

in their sensor models. In practice, the thin film is usually supported by a massive silicon (Si) substrate, where the bulk Si is a good heat conductor with a thermal conductivity around 150W/(m·K). Therefore, the temperature of thin film is expected to be equal to ambient temperature T_a at a finite distance from the micro heater, i.e. at the supporting ends.

In this paper, we extended our previous TMCF sensor model [14] to a general 1D model for two types of sensor packaging: open-space type and channel-type, as shown in Fig. 1. The proposed model enables the rapid analysis of sensitivity and power consumption as functions of key design parameters such as the distance between the micro heater and thermoresistive sensors, the thickness of the thin film, and the height of the bottom cavity. According to such design analysis for the bare sensor chip, TMCF sensors were fabricated by a 0.35μm 2P4M CMOS MEMS technology. The packaged TMCF sensors showed an excellent normalized sensitivity of 230mV/(m/s)/mW, which was two orders of magnitude better than those reported in the literature [15]–[17]. Besides, the measured sensor response curves were in good agreement with the theoretical prediction of 1D model.

II. THEORETICAL MODEL OF TMCF SENSORS

As shown in Fig. 1(b), a TMCF sensor usually consists of a micro-heater at the center of a thin film, and two symmetrically located upstream and downstream thermoresistive sensors with the output of temperature T_u and T_d, respectively. In the absence of input fluid flow, the overheated temperature profile $T(x)$ of a TMCF sensor in the streamwise (x) direction is symmetrically distributed. In the presence of input fluid flow, the differential temperature output ($\Delta T = T_d - T_u$) of the TMCF sensor can be monitored and related to the input flow velocity U through the micro convective heat transfer.

Instead of solving the nonlinear coupled partial differential equations of fluid mechanics and heat transfer, the lumped parameter method was employed to describe the key behavior of TMCF sensors. The temperature profile in the y direction of fluids and the thin film was assumed to be piecewise linear while the temperature profile in the direction perpendicular to the x-y plane (z-axis) was ignored. Therefore, the originally required three-dimensional (3D) heat transfer analysis can be reduced to a simple one-dimensional (1D) one, i.e. only in the streamwise (x) direction. As shown in Fig. 1(c), in the steady state, the sum of the incoming convective and conductive heat fluxes in a control volume of $\Delta x \times y \times 1$ excluding the micro heater region is equal to the sum of the outgoing heat fluxes as follows:

$$Q_{f,x}^{cond} + Q_{f,x}^{conv} + Q_{s,x}^{cond} + Q_{f1,x}^{cond} = Q_{f,y}^{cond} + Q_{f1,y}^{cond} \quad (1)$$

where the subscripts, s, f, and $f1$, denote the solid thin film, the fluid on the top, and the fluid on the bottom of thin film, respectively; the superscripts, *cond* and *conv*, denote heat conduction and heat convection, respectively.

For a control volume in Fig. 1(c), the accumulated incoming and outgoing conductive heat fluxes can be calculated as:

$$\begin{aligned} Q_{s,x}^{cond} &= k_s\frac{d^2T(x)}{dx^2}\Delta xt \\ Q_{f,x}^{cond} &= \frac{1}{2}k_f\frac{d^2T(x)}{dx^2}\Delta x\delta_{t,x} \\ Q_{f1,x}^{cond} &= \frac{1}{2}k_{f1}\frac{d^2T(x)}{dx^2}\Delta xh \\ Q_{f,y}^{cond} &= k_f\frac{T(x)}{\delta_{t,x}}\Delta x \\ Q_{f1,y}^{cond} &= k_{f1}\frac{T(x)}{h}\Delta x \end{aligned} \quad (2)$$

The incoming convective heat flux is expressed by (3) for the open-space type sensor, where the linear flow velocity profile is assumed within the momentum boundary layer.

$$Q_{f,x}^{conv} = \frac{\rho C_PU\delta_{t,x}^2}{6\delta_x}\frac{dT(x)}{dx}\Delta x \quad (3)$$

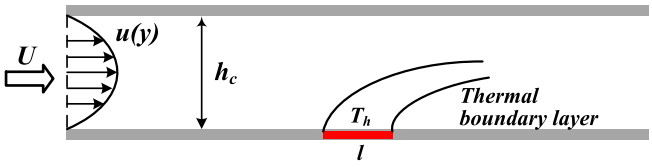

Fig. 2. Schematic view of the developed thermal boundary layer, $\delta_{t,x}$, of a partially heated area (l) within a flow channel, $l = 2L$ (Fig.1).

While for the channel-type sensor with the developed parabolic flow velocity profile [18], the incoming convective heat flux is expressed by (4).

$$Q_{f,x}^{conv} = \rho C_P U \frac{dT(x)}{dx}\left(\frac{\delta_{t,x}^2}{h_c} - \frac{\delta_{t,x}^3}{2h_c^2}\right)\Delta x \tag{4}$$

The symbols in (2), (3) and (4) are: h is the cavity height, t is the thin film thickness, k_s, k_f and k_{f1} are the thermal conductivity of the thin film, the moving fluid on the top of the thin film, and the fluid in the cavity, respectively. ρ and C_p are the density and heat capacity of the moving fluid, respectively. δ_x is momentum boundary layer, $\delta_{t,x}$ is thermal boundary layer, h_c is the height of flow channel in channel-type design.

By substituting (2), (3) or (4) into (1), and considering the averaged momentum boundary layer δ and thermal boundary layer δ_t, the nonlinear governing equation of TMCF sensors can be reduced to a linearized 1D model.

$$\left(k_s t + \frac{1}{2}k_f\delta_t + \frac{1}{2}k_{f1}h\right)\frac{d^2T(x)}{dx^2} - \rho C_P U\beta_i\frac{dT(x)}{dx} - \left(\frac{k_f}{\delta_t} + \frac{k_{f1}}{h}\right)T(x) = 0; \quad i = 1,\ 2 \tag{5}$$

β_i is the coefficient of packaged sensor type. In details, β_1 is for open-space type sensor, and β_2 is for channel-type sensor.

$$\beta_1 = \frac{\delta_t^2}{6\delta};\ \beta_2 = \left(\frac{\delta_t^2}{h_c} - \frac{\delta_t^3}{2h_c^2}\right) \tag{6}$$

For the open-space type sensor, the averaged momentum boundary layer δ along the thin film can be calculated by integrating (7) along the x-axis [19].

$$\delta_x = 4.64\sqrt{\frac{\mu_f(x+s)}{\rho U}} \tag{7}$$

μ_f is the dynamic viscosity of the moving fluid, and $2s$ is the length of bare TMCF sensor chip. Then, the averaged thermal boundary layer δ_t can be determined as [19].

$$\delta_t = \zeta\delta;\ \zeta = \frac{1}{1.026}Pr^{-1/3}\left[1 - \left(1 - \frac{L}{s}\right)^{3/4}\right]^{1/3} \tag{8}$$

where Pr is the Prandtl number defined as the ratio of the momentum diffusivity to thermal diffusivity.

For the channel-type sensor with the channel height of h_c, the parabolic velocity profile is assumed for the fully developed flow [18], as shown in Fig. 2. For the case of h_c larger than $\delta_{t,x}$ or the Prandtl number of fluid (Pr) larger than 1, the developed thermal profile can be fitted by a cubic polynomial [19]. Therefore, based on the principle of energy conservation, we have:

$$\frac{d}{dx}\int_0^{\delta_{t,x}} TU_y dy = T_h\frac{6U}{h_c^2} \cdot \frac{d}{dx}\left[\int_0^{\delta_{t,x}}\left(1 - \frac{3}{2}\frac{y}{\delta_{t,x}} + \frac{1}{2}\left(\frac{y}{\delta_{t,x}}\right)^3\right)\left(h_c y - y^2\right)dy\right] = \frac{3\alpha_k T_h}{2\delta_{t,x}} \tag{9}$$

where α_k is the thermal diffusivity. Ignoring the high order term of $\delta_{t,x}/h_c$ in (9), the solution of thermal boundary layer $\delta_{t,x}$ is:

$$\delta_{t,x} = h_c\left(\frac{15}{4Re_c Pr}\frac{x}{h_c}\right)^{1/3} x = 0\ to\ l \tag{10}$$

where the channel Reynolds number is defined as $Re_c = \rho U h_c/\mu_f$ [18], then the averaged thermal boundary layer δ_t is calculated as:

$$\delta_t = \frac{\int_0^l \delta_{t,x}dx}{l} = 1.17h_c\left(\frac{l}{h_c Re_c Pr}\right)^{1/3} \tag{11}$$

where l is the partially heated length, with the assumption of isothermal thin film for TMCF sensor, we have $l = 2L$ in this paper. For the case of small Re_c flow, the thickness of δ_t could be simply regarded as the height of h_c [13]. Note that if we neglect the heat conduction in the bottom cavity and make $\delta_t = h_c$, our 1D model in (5) is simplified to Nguyen's model [13]:

$$\left(k_s t + \frac{1}{2}k_f\delta_t\right)\frac{d^2T(x)}{dx^2} - \frac{\rho C_P U\delta_t}{2}\frac{dT(x)}{dx} - \frac{k_f T(x)}{\delta_t} = 0 \tag{12}$$

For the design of CMOS TMCF sensors, the thin film is usually supported on a bulk silicon (Si) substrate, where the bulk Si has a thermal conductivity around 150W/(m·K). Therefore, we can expect the temperature of thin film at both supporting ends to be equal to the ambient temperature T_a. For the simplicity of calculation, the overheated temperature $T_h = Tw - T_a$ is adopted, where Tw is the working temperature of micro heater.

$$T(-L) = 0,\ T(-W) = T_h;\ T(L) = 0,\ T(W) = T_h \tag{13}$$

Applying four thermal boundary conditions of (13) into (5), we can determine the analytical solution of temperature profile $T(x)$ in the streamwise (x) direction as follows:

$$\begin{cases} T(x) = \dfrac{T_h\left(e^{r_2 x} - e^{-r_2 L + r_1(x+L)}\right)}{e^{-r_2 W} - e^{-r_2 L - r_1(W-L)}};\ -L \leqslant x < -W \\ T(x) = T_h;\ -W \leqslant x \leqslant W \\ T(x) = \dfrac{T_h\left(e^{r_2 x} - e^{r_2 L + r_1(x-L)}\right)}{e^{r_2 W} - e^{r_2 L + r_1(W-L)}};\ W < x \leqslant L \end{cases} \tag{14}$$

r_1 and r_2 are the eigenvalues of the linearized governing equation (5):

$$r_1 = \frac{-B + \sqrt{B^2 - 4AC}}{2A};\ r_2 = \frac{-B - \sqrt{B^2 - 4AC}}{2A} \tag{15}$$

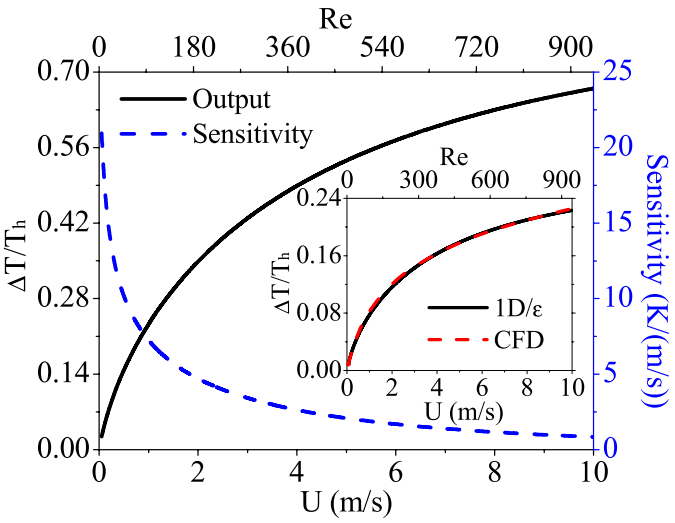

Fig. 3. The TMCF sensor's mechano-thermal sensitivity and normalized output as a function of input air flow velocity U and Re. The inset shows the comparison of the sensor output between CFD and 1D model. ($2s = 1500\mu$m, $2L = 600\mu$m, $2W = 100\mu$m, $D = 120\mu$m, $h = 150\mu$m, $t = 4\mu$m).

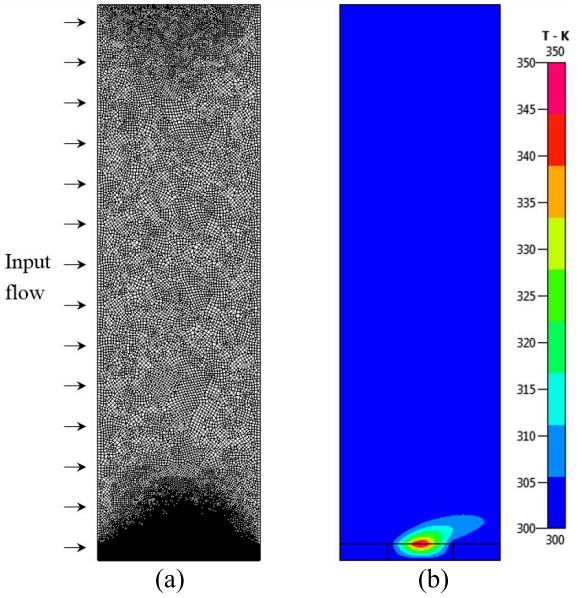

Fig. 4. (a) The numerical model for the open-space packaged TMCF sensor with 50,140 cells, (b) the distribution of simulated temperature profile under the input air flow velocity of 1m/s.

where A, B, and C are the coefficients:

$$A = \left(k_s t + \frac{1}{2}k_f \delta_t + \frac{1}{2}k_{f1} h\right)$$
$$B = -\rho C_P U \beta_i$$
$$C = -\left(\frac{k_f}{\delta_t} + \frac{k_{f1}}{h}\right) \tag{16}$$

Assuming two thermoresistive sensors as point sensors at $x = D + W$ and $x = -D - W$, the thermal output ΔT of TMCF sensor can be determined as:

$$\Delta T = T\,(D + W) - T\,(-D - W) \tag{17}$$

By differentiating the sensor output ΔT in (17) with respect to the input fluid flow velocity U, we can determine the mechano-thermal sensitivity $S_m = d(\Delta T)/dU$, while the power consumption of TMCF sensor P is determined as the sum of heat loss from the interfaces of the micro heater.

With the help of dimensional analysis [18], the TMCF sensor output ΔT can be normalized with the overheat temperature T_h as a function of Reynolds number (Re) and Prandtl number (Pr) for both gases and liquids as shown in (18). The dimensionless input flow parameter (related to the normalized velocity and thermal properties) $\phi_1 = Re^{1/2}Pr^{1/3}$ is used in the open-space type sensor with the local Reynolds number defined as $Re = 2\rho U s/\mu_f$, while $\phi_2 = Re_c Pr$ is adopted in the channel-type sensor with the channel Reynolds number defined as $Re_c = \rho U h_c/\mu_f$ [18]. More details of the 1D model that applied to an open-space type sensor have been reported and validated in our previous paper [14].

$$\Delta T/T_h = f\left(\phi_j,\ k_f^*\right);\quad j = 1,\ 2 \tag{18}$$

III. Analysis of 1D Model

A. Comparison With Numerical Simulations

The predicted sensitivity S_m and normalized output $\Delta T/T_h$ as a function of input air flow velocity U and Re for the open-space type sensor are shown in Fig. 3, where the dimensions of the sensor are listed in the caption of Fig. 3. The heater works on Constant Temperature Difference (CTD) mode with $T_h = 50$K. The thin film is mainly composed of a silicon oxide layer with a nominal thermal conductivity k_s of 1.4W/m/K. As depicted in Fig. 3, the output ΔT increases with the increased fluid flow, while the sensitivity S_m decreases. This phenomenon indicates that there is a trade-off between the output amplitude and the sensitivity. In general, highly sensitive TMCF sensor can be achieved at small input flow, which allows the application of micro calorimetric flow sensors in low flow velocity measurements.

Previously, we constructed a CFD model which can predict the response of a TMCF sensor in [20], and demonstrated the capability of the CFD model in the prediction of different TMCF sensors' response [14]. Herein, with the presented TMCF sensor structure in design stage, a 2D CFD model (CFD-ACE+, ESI CFD Inc., USA) was built. The cross section of the thin film TMCF sensors was approximated by a rectangular area with the averaged thermal properties. A total number of 50,140 cells were achieved in the simulation domain with the enough open-space as shown in Fig. 4(a). The numerical simulation only contains the heat conduction and the heat convection, where the radiative heat transfer and the natural convection were ignored. Fig. 4(b) shows the asymmetric thermal distribution of TMCF sensors under the input air flow velocity of 1m/s.

In the inset of Fig. 3, the simulated thermal output ΔT of TMCF sensors as a function of input air flow velocity is plotted. Good agreement between the 1D model results with a fitting factor ε of 3 and the 2D CFD results is observed in the inset of Fig. 3, which demonstrates that our 1D model can qualitatively predict sensor response, and significantly save the CPU time with a factor of 100,000. The 1D model with

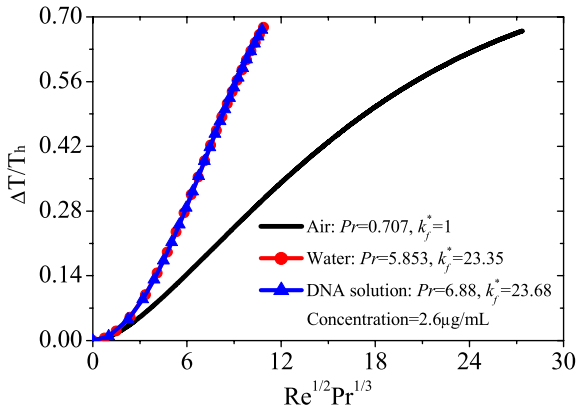

Fig. 5. Normalized output of TMCF sensor for air, water and DNA solution. Note: the parameters (S, L, W, h, D, t) are the same as Fig. 3.

the correction of a fitting factor can be regarded as a semi-empirical TMCF model. The reason for introducing a fitting factor is mainly from the assumption of the simplified average thermal boundary layer δ_t over the assumed isothermal thin film. In this case, the heat convection in a control volume is *underestimated* in the upstream area of thin film, while the heat convection is *overestimated* in the downstream area. Therefore, the calculated differential thermal output of TMCF sensor in the 1D model is larger than that of CFD simulation. More sophisticated modeling of the TMCF sensor is in progress to solve the issue of fitting factor. Fig. 5 shows the normalized sensor output $\Delta T/T_h$ as a function of normalized velocity input ϕ for air, water, and one representative biofluid of DNA solution (2.6μg/mL), which demonstrates that our 1D model can be applied to different types of fluids.

B. Design Analysis of CMOS TMCF Sensors

Fig. 6 shows the scaling analysis of the predicted key merits for the bare CMOS TMCF sensors, including sensor output and sensitivity. An optimal distance ($D/L = 0.3 \sim 0.4$) between the heater and temperature sensor could achieve the largest output in the flow range of 0-10m/s for the open-space type sensor, as shown in Fig. 6(a). Note, in consideration of the finite size of micro heater ($W = 50\mu$m), the maximum value of D/L is 0.833. Meanwhile, to achieve a better sensor output and sensitivity for the detection of higher speed fluids flow, one should place the thermoresistive sensors close to the micro heater, as shown in Fig. 6(a) and Fig. 6(b), respectively. Similar behavior of TMCF sensors in the CFD model could also be observed.

Fig. 7(a) reveals that a thinner film design can help the TMCF sensor achieve a lower power consumption and higher sensitivity. It should be noted that the CMOS fabrication process and the mechanical strength of materials limit the minimum thickness of thin film. One more thing to be pointed out is that the thermal conductivity k_s of CMOS oxide appears to be widely different from 1 to 1.6 W/m/K due to the highly process depended microstructure [21]. Moreover, after the post-CMOS process of the TMCF sensors, the released thin film structures would be composed of silicon oxide, poly-Si, metal material, etc. Typically, poly-Si and metal materials

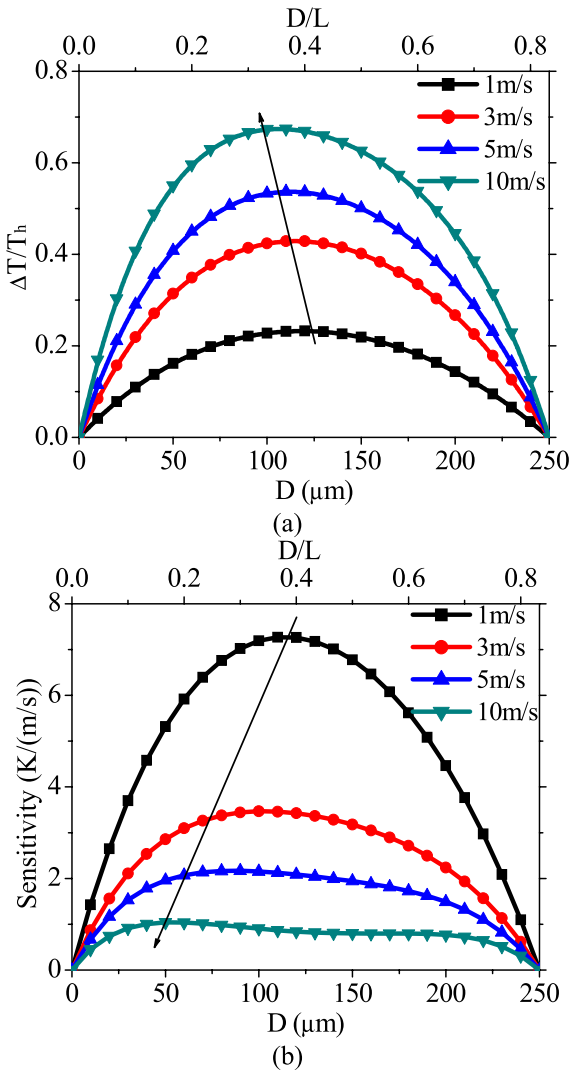

Fig. 6. The effect of distance between the heater and sensing elements (D) on the sensor's (a) normalized output and (b) mechano-thermal sensitivity. Note: the remaining parameters are the same as Fig. 3.

in CMOS ICs have a thermal conductivity around one and two orders of magnitude higher than that of silicon oxide, respectively [21]. Therefore, we may expect an even higher averaged thermal conductivity of thin film in the CMOS TMCF sensors. As shown in Fig. 7(b), it makes clear that the predicted CMOS TMCF sensors' performance is dramatically decreased with the increased thermal conductivity k_s of the thin film materials. Therefore, to achieve better prediction and design of integrated on-chip thermal flow sensors, it is crucial to have precise knowledge and measurements of thin films' thermal properties in a specified CMOS fabrication process.

Further parametric study of the bottom cavity height h on the sensor's behavior in Fig. 8 suggests a height of h/L larger than 0.11 ($h > 33\mu$m) to achieve a better sensor performance. The optimization of this bottom cavity height is also necessary for a proper sensor design without requiring a long time post-CMOS fabrication process.

IV. Fabrication and Test of TMCF Sensor

Based on the design analysis for bare sensor chip, three pairs of TMCF sensors (Pair 1-3) at different locations, $D = 60\mu$m,

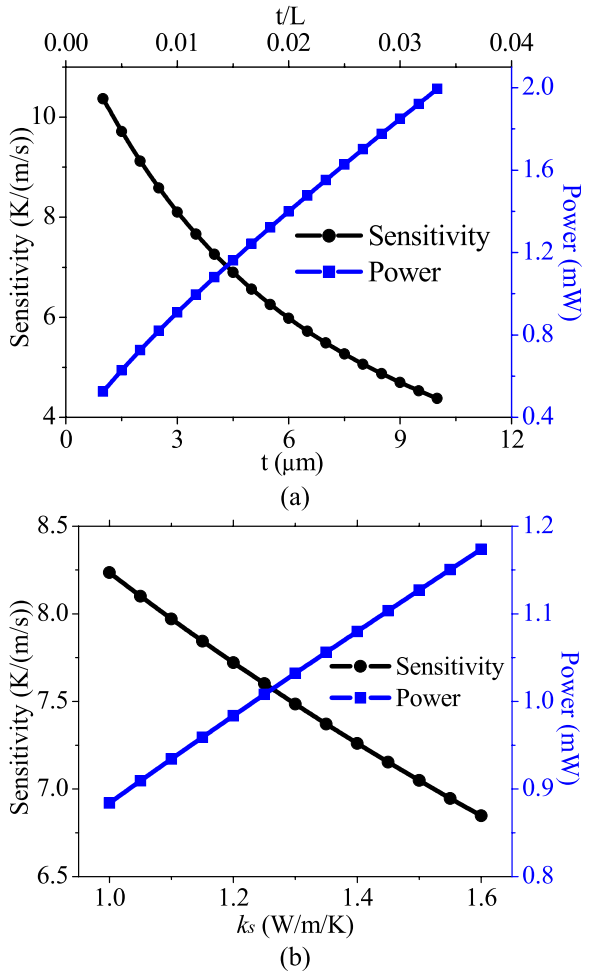

Fig. 7. The effects of thin film (a) thickness t and (b) thermal conductivity k_s on the sensor's power consumption and mechano-thermal sensitivity at $U = 1$m/s. Note: the remaining parameters are the same as Fig. 3.

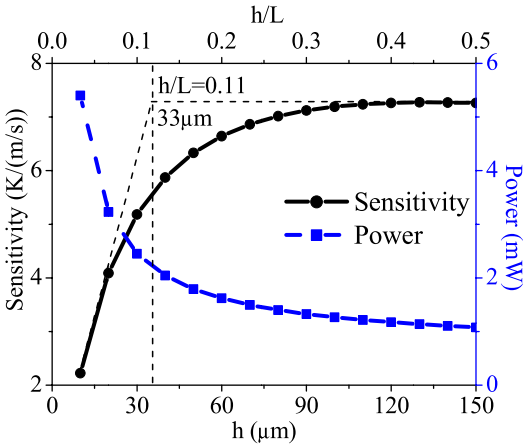

Fig. 8. The effects of bottom cavity height h on the sensor's power consumption and mechano-thermal sensitivity at $U = 1$m/s. Note: the remaining parameters are the same as Fig. 3.

120μm, 180μm were designed and fabricated by a commercial 0.35μm 2P4M CMOS MEMS process. The PAD layer in the CMOS process was used to define the 600μm $\times$ 400μm MEMS opening structure. Then, the selective oxide reactive ion etching (RIE) was used to define the sensor structure, and the XeF_2 isotropic Si etching was used to release the 3.6μm thick oxide based thin film structure with the bottom cavity h around 40μm as shown in Fig. 9. An optical micrograph of the fabricated TMCF sensor is shown in Fig. 10(a). The polysilicon resistors were determined to have a temperature coefficient of resistance (TCR) $\alpha = 8.52 \times 10^{-4}$ K^{-1}. The TMCF sensors were then embedded in a PCB board and packaged in a machined PMMA flow channel with the channel size of 80mm $\times$ 8mm $\times$ 4mm (Length $\times$ Width $\times$ Height). The PMMA flow channel was bonded with PCB board by eight bolts and sealed with an O-Type seal ring as shown in Fig. 10(b).

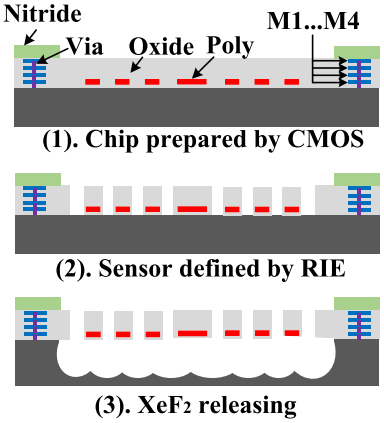

Fig. 9. Post-CMOS process for the releasing of TMCF sensor structure.

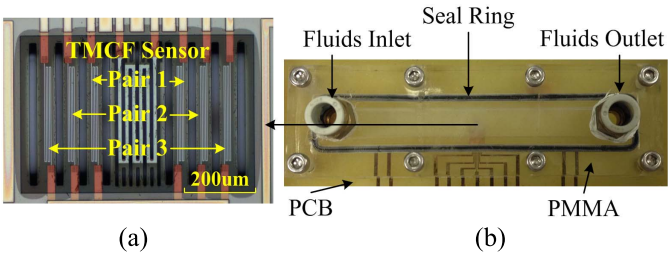

Fig. 10. (a) Optical micrograph of a fabricated TMCF sensor, (b) Packaged TMCF sensor in a PMMA flow channel.

The normalized 1D model demonstrated that the thermal output ΔT has a linear relationship with the overheated temperature T_h. Thus, with the micro heater working on CTD mode, an ambient temperature T_a compensated TMCF sensor could be realized. The T_a compensated circuit for the TMCF sensor was constructed as shown in Fig. 11, in which the micro heater works on CTD mode with $T_h = 50$K. More details of this temperature compensated TMCF sensor design could be found in our previous paper [22]. The packaged TMCF sensors were then tested with nitrogen flow as shown in Fig. 12. The nitrogen tank ($P_{max} = 15$bar) was used as the gas source, and a commercial flow sensor AWM5104VN (Honeywell, USA) was used as a reference flow meter.

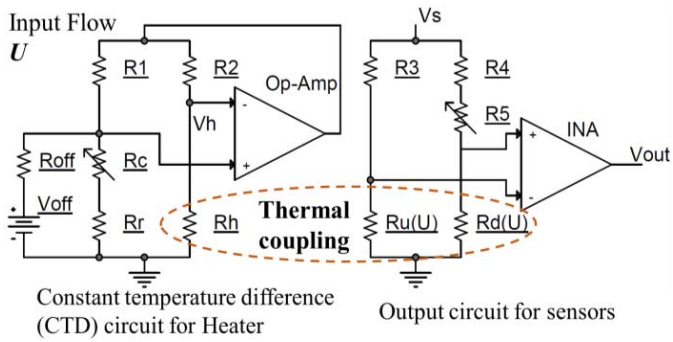

Fig. 11. The ambient temperature-compensated circuit for TMCF sensors with the reference temperature sensor R_T and the compensation resistor R_C [22].

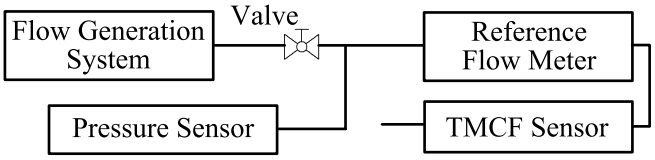

Fig. 12. Experimental setup for the testing of TMCF sensor.

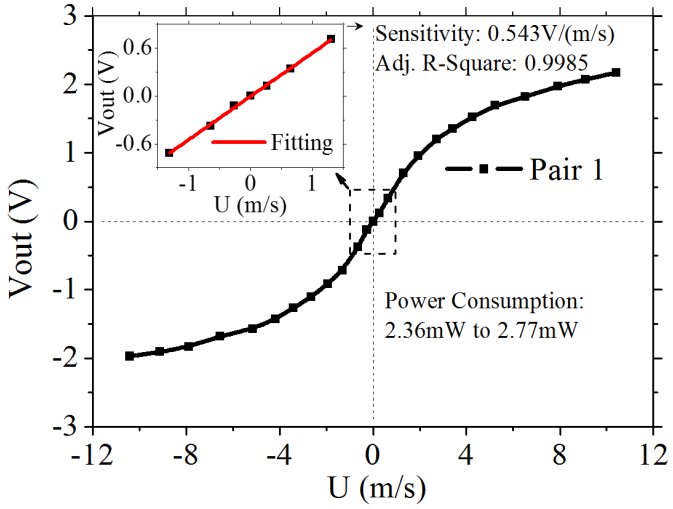

Fig. 13. The measured output voltage of the fabricated Pair 1 TMCF sensor under CTD mode as a function of input flow velocity (−11m/s-11m/s). The overheated temperature T_h is 50K. The sensitivity of the sensor determined in low flow region is very large, 0.543V/(m/s).

V. Discussion

The symmetric sensor output of Pair 1 TMCF sensor was observed without saturation, as shown in Fig. 13, which demonstrated that our TMCF sensor is capable for bidirectional flow detection with the N_2 gas flow from −11m/s to 11m/s. Meanwhile, this sensor design had a low-power consumption (2.36mW∼2.77mW) and high sensitivity (0.543V/(m/s)). To compare its performance to those CMOS calorimetric flow sensors reported in the literature, we normalized the sensitivity with respect to the applied heating power. As revealed in Table II, the normalized sensitivity of our TMCF sensor (230 mV/(m/s)/mW) was about two orders of magnitude larger than those of the other flow sensors.

TABLE II
Comparisons Between the Reported CMOS Calorimetric Flow Sensor and Our Work

Reference	*DS*, mm^2	*F*	*FR*, m/s	*P*, mW	*S**, mV/(m/s)/mW
Bruschi[15, a]	16	N_2	-3.33-3.33	4	2.3
Dong[16, b]	36	Air	0.5-40	2-452.6	3.93
Moser[17, a]	N/A	N_2	0 - 85	13	4.24
Mayer[24, a]	18	Air	0.02-38	3	N/A
Makinwa[25, a]	16	Air	2 - 18	400-600	N/A
Wu[26, a]	16	Air	1 - 25	25	N/A
Our work[b]	2.25	N_2	-11-11	2.36-2.77	230

[a] thermopile transduction principle, [b] thermoresistive transduction principle. *DS* = Die Size, *F* = Fluids, *FR* = Flow Range, *P* = Power, *S** = Sensitivity normalized with respect to input power.

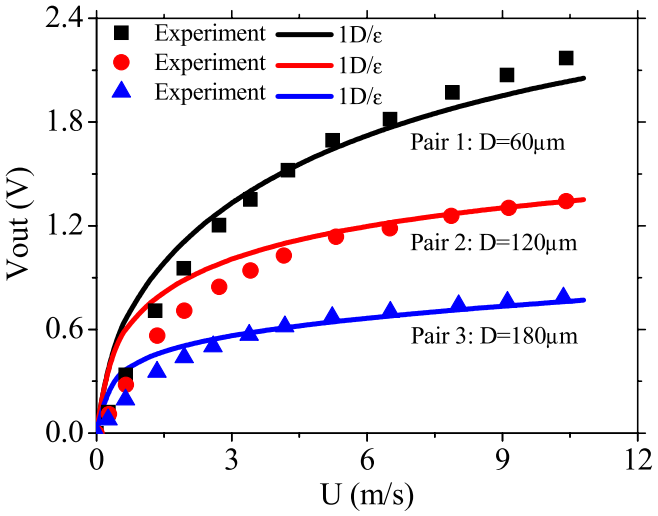

Fig. 14. Comparison of the measured three pairs of TMCF sensors responses (markers) with the predicted curves from 1D model (solid line).

The opening area in the thin film of TMCF sensors is sparse. Therefore, as it is confirmed by CFD simulation, the bottom cavity N_2 gas flow in the TMCF sensors can be ignored. Previously, we found that the developed flow pattern in flow channel could cause a profound impact on the TMCF sensors' performance [23], and a much more comprehensive study of this effect will be conducted later. Herein, for ease of theoretical analysis, especially for the high Re_c flow, a fully developed parabolic velocity profile over the TMCF sensor chip is assumed. Therefore, the packaged CMOS TMCF sensors' response can be predicted by our 1D model (channel-type) with the averaged thermal properties of the thin film. With the applied interface circuit of Wheatstone bridge for the upstream and downstream thermoresistive sensors as shown in Fig. 11, the electrical output V_{out} of the TMCF sensor is monitored as a linear function of the thermal output ΔT [22]. Similar to the experimental results, 1D model (a fitting factor ε of 3.8 for all three pairs of TMCF sensors) depicts the same trend that the sensing elements close to heater could gain a larger output and sensitivity, as shown in Fig. 14. Apparently, the general behavior of TMCF sensors can be predicted by our

1D analysis. As supported by the experimental results, the proposed general 1D model is validated with the introduction of a semi-empirical fitting factor ε.

VI. Conclusion

In summary, we successfully fabricated the TMCF sensors by a 0.35μm 2P4M CMOS MEMS process and proposed a general 1D model of TMCF sensors for two types of packaging designs: the open-space type and the channel-type. With the help of dimensional analysis, the normalized sensor model can be applied to both gases and liquids. Detailed investigation of TMCF sensor's sensitivity and power consumption as a function of dimensionless geometric parameters for the 0.35μm 2P4M CMOS MEMS process were performed. Based on this design analysis, the optimal CMOS TMCF sensor designs were determined. Accordingly, the fabricated CMOS TMCF sensors achieved a normalized sensitivity of 230mV/(m/s)/mW for the nitrogen gas flow, which was two orders of magnitude higher than the previous CMOS flow sensors. Besides, with the introduction of a semi-empirical fitting factor ε, the responses of TMCF sensors predicted by our 1D model (1D/ε) were in good agreement with the experimental data. Therefore, our 1D model is useful for the efficient system-level design of new TMCF sensors with the integrated on-chip microelectronics, such as the signal conditioning circuit, Operational Amplifier, Analog-to-Digital Converter, and so on for Internet of Things (IoT).

Acknowledgment

The authors acknowledge the technical support of Mr. W. L. Yeung and the staff at HKUST NFF and MCPF.

References

[1] A. F. P. Van Putten and S. Middelhoek, "Integrated silicon anemometer," *Electron. Lett.*, vol. 10, no. 21, pp. 425–426, Oct. 1974.

[2] S. Silvestri and E. Schena, "Micromachined flow sensors in biomedical applications," *Micromachines*, vol. 3, no. 2, pp. 225–243, Mar. 2012.

[3] N. T. Nguyen, "Micromachined flow sensors—A review," *Flow Meas. Instrum.*, vol. 8, no. 1, pp. 7–16, Mar. 1997.

[4] Y.-H. Wang *et al.*, "MEMS-based gas flow sensors," *Microfluidics Nanofluidics*, vol. 6, no. 3, pp. 333–346, Jan. 2009.

[5] J. T. W. Kuo, L. Yu, and E. Meng, "Micromachined thermal flow sensors—A review," *Micromachines*, vol. 3, no. 3, pp. 550–573, Jul. 2012.

[6] F. Hedrich, K. Kliche, M. Storz, S. Billat, M. Ashauer, and R. Zengerle, "Thermal flow sensors for MEMS spirometric devices," *Sens. Actuators A, Phys.*, vol. 162, no. 2, pp. 373–378, Mar. 2010.

[7] Z. Miao, C. Y. H. Chao, Y. Chiu, C.-W. Lin, and Y.-K. Lee, "Design and fabrication of micro hot-wire flow sensor using 0.35 μm CMOS MEMS technology," in *Proc. Nano/Micro Eng. Molecular Syst. (NEMS)*, Waikiki Beach, HI, USA, Apr. 2014, pp. 289–293.

[8] A. Persson, V. Lekholm, G. Thornell, and L. Klintberg, "A high-temperature calorimetric flow sensor employing ion conduction in zirconia," *Appl. Phys. Lett.*, vol. 106, no. 19, p. 194103, May 2015.

[9] W. Fang *et al.*, "CMOS MEMS: A key technology towards the 'more than Moore' era," in *Proc. Int. Solid-State Sens., Actuators, Microsyst. Conf. (TRANSDUCERS)*, Barcelona, Spain, Jun. 2013, pp. 2513–2518.

[10] F. Mayer, G. Salis, J. Funk, O. Paul, and H. Baltes, "Scaling of thermal CMOS gas flow microsensors: Experiment and simulation," in *Proc. IEEE 9th Annu. Int. Workshop Micro Electro Mech. Syst. (MEMS), Invest. Micro Struct., Sens., Actuators, Mach. Syst.*, San Diego, CA, USA, Feb. 1996, pp. 116–121.

[11] K. Komiya, F. Higuchi, and K. Ohtani, "Characteristics of a thermal gas flowmeter," *Rev. Sci. Instrum.*, vol. 59, no. 3, pp. 477–479, Mar. 1988.

[12] T. S. J. Lammerink, N. R. Tas, M. Elwenspoek, and J. H. J. Fluitman, "Micro-liquid flow sensor," *Sens. Actuators A, Phys.*, vol. 37–38, pp. 45–50, Jun./Aug. 1993.

[13] N. T. Nguyen and W. Dötzel, "Asymmetrical locations of heaters and sensors relative to each other using heater arrays: A novel method for designing multi-range electrocaloric mass-flow sensors," *Sens. Actuators A, Phys.*, vol. 62, nos. 1–3, pp. 506–512, Jul. 1997.

[14] W. Xu, K. Song, S. Ma, Y. Chiu, and Y. Lee, "One dimensional model of thermoresistive micro calorimetric flow (TMCF) sensors for gases and liquids considering Prandtl number effect," in *Proc. 18th Int. Conf. Miniaturized Syst. Chem. Life Sci., (MicroTAS)*, San Antonio, TX, USA, Oct. 2014, pp. 2333–2335.

[15] P. Bruschi, M. Dei, and M. Piotto, "A single chip, double channel thermal flow meter," *Microsyst. Technol.*, vol. 15, no. 8, pp. 1179–1186, Aug. 2009.

[16] Z. Dong, J. Chen, Y. Qin, M. Qin and, and Q.-A. Huang, "Fabrication of a micromachined two-dimensional wind sensor by Au–Au wafer bonding technology," *J. Microelectromech. Syst.*, vol. 21, no. 2, pp. 467–475, Apr. 2012.

[17] D. Moser and H. Baltes, "A high sensitivity CMOS gas flow sensor on a thin dielectric membrane," *Sens. Actuators A, Phys.*, vol. 37–38, pp. 33–37, Jul./Aug. 1993.

[18] M. C. Potter, D. C. Wiggert, and B. H. Ramadan, *Mechanics of Fluids*, 4th ed. Stamford, CT, USA: Cengage Learning, 2011.

[19] J. Holman, *Heat Transfer*, 9th ed. New York, NY, USA: McGraw-Hill, 2002.

[20] F. Kohl, R. Fasching, F. Keplinger, R. Chabicovsky, A. Jachimowicz, and G. Urban, "Development of miniaturized semiconductor flow sensors," *Measurement*, vol. 33, no. 2, pp. 109–119, Mar. 2003.

[21] A. Nathan and H. Baltes, *Microtransducer CAD: Physical and Computational Aspects*. New York, NY, USA: Springer, 1999.

[22] W. Xu, B. Gao, S. Ma, A. Zhang, Y. Chiu, and Y.-K. Lee, "Low-cost temperature-compensated thermoresistive micro calorimetric flow sensor by using 0.35 μm CMOS MEMS technology," in *Proc. 25th IEEE Int. Conf. Micro Electro Mech. Syst. (IEEE MEMS)*, Shanghai, China, Jan. 2016, pp. 189–192.

[23] W. Xu, B. Gao, Y. Chiu, and Y.-K. Lee, "Packaging effect on the flow separation of CMOS thermoresistive micro calorimetric flow sensors," in *Proc. 11th Annu. IEEE Int. Conf. Nano/Micro Eng. Molecular Syst. (IEEE-NEMS)*, Matsushima Bay and Sendai, Japan, Apr. 2016, pp. 1–4.

[24] F. Mayer, A. Haberli, H. Jacobs, G. Ofner, O. Paul, and H. Baltes, "Single-chip CMOS anemometer," in *IEDM Tech. Dig.*, Washington, DC, USA, Dec. 1997, pp. 895–898.

[25] K. A. A. Makinwa and J. H. Huijsing, "A smart wind sensor using thermal sigma-delta modulation techniques," *Sens. Actuators A, Phys.*, vols. 97–98, pp. 15–20, Apr. 2002.

[26] J. Wu, C. van Vroonhoven, Y. Chae, and K. Makinwa, "A 25mW CMOS sensor for wind and temperature measurement," in *Proc. IEEE Sensors*, Limerick, Republic of Ireland, Oct. 2011, pp. 1261–1264.

Wei Xu received the B.S. and M.S. degrees in materials processing engineering from the Huazhong University of Science and Technology, Wuhan, China, in 2010 and 2013, respectively. He is currently pursuing the Ph.D. degree in mechanical and aerospace engineering at the Hong Kong University of Science and Technology, Hong Kong.

His research interest includes the heat/mass transfer, fluid mechanics, material processing and simulation and equipment, micro/nano fabrication technology, CMOS MEMS sensors, and micro/nanofluidics.

Kui Song received the bachelor's degree in engineering and mechanics from Xiangtan University, and the Ph.D. degree in fluid mechanics from the Institute of Mechanics, Chinese Academy of Sciences.

He is currently a Lecturer with Xiangtan University. He is a Visiting Scholar with the Hong Kong University of Science and Technology. His research work is about microfluidics and MEMS sensors. He did research work on the logic function of droplet microfluidics, droplet-based microfluidics, and microfluidic chip applications.

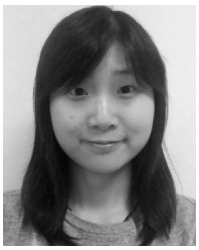

Shenhui Ma received the B.S. degree in microelectronics from Xi'an Jiaotong University, Xi'an, China, in 2013. She is currently pursuing the Ph.D. degree in the joint dual-degree Ph.D. program at Xi'an Jiaotong University and the Hong Kong University of Science and Technology, Hong Kong.

Her research interests include micro/nano fabrication technology, microelectronics devices, and micro/nano electrochemical biosensors.

Bo Gao received the B.S. degree in microelectronics from Xi'an Jiaotong University, Xi'an, China, in 2014. She is currently pursuing the Ph.D. degree in bioengineering at the Hong Kong University of Science and Technology, Hong Kong.

Her research interests include the electrochemical processes, micro/nano electrochemical biosensors, microelectronics devices, and MEMS sensors.

Yi Chiu received the B.S. degree in electrical engineering from National Taiwan University, Taiwan, ROC, in 1988, and the M.S. and Ph.D. degrees in electrical and computer engineering from Carnegie Mellon University, Pittsburgh, PA, USA, in 1991 and 1996, respectively.

He was at Acer Media Technology (now BenQ Materials) from 1998 to 2001, and worked on advanced optical storage media. He is currently a Professor with the Department of Electrical and Computer Engineering, National Chiao Tung University, Taiwan. His research interests include energy harvesting, optical MEMS, and CMOS-MEMS sensors.

Yi-Kuen Lee received the B.S. degree (Hons.) in biomechatronic industrial engineering and the M.S. degree in applied mechanics form National Taiwan University, and the Ph.D. degree in MEMS from the University of California, Los Angeles, in 2001.

He is currently an Associate Professor with the Department of Mechanical and Aerospace Engineering, and the Division of Biomedical Engineering, Hong Kong University of Science and Technology. He was a Visiting Associate at Caltech from 2010 to 2011. He was the President of the Hong Kong Society of Theoretical and Applied Mechanics from 2014 to 2016. His current research focuses on microfluidics for the enumeration of circulation tumor cells for cancer diagnostics, microchips for DNA transfection, micro/nano heat transfer, micro/nano electrokinetic devices for manipulations of DNA molecules and cells, MEMS sensors for environmental monitoring, and energy-efficiency building. He co-founded the Annual Nano/Micro Engineered and Molecular Systems (IEEE NEMS) Conference.